Analyst

Accepted Manuscript

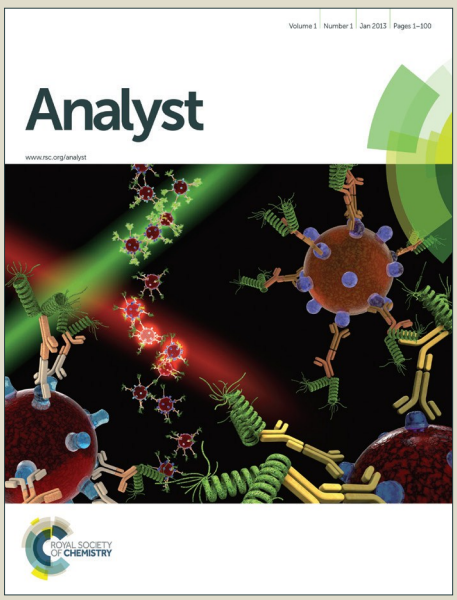

ROYAL SOCIETY OF CHEMISTRY

www.rsc.org/analyst

Anti-CD155 and anti-CD112 monoclonal antibodies conjugated to a fluorescent mesoporous silica nanosensor encapsulating rhodamine 6G and fluorescein for sensitive detection of liver cancer cells

Liang Tao[a, b, 1], Chaojun Song[a, 1], Chenyang Huo [d, 1], Chunmei Zhang[a], Yuanjie Sun[a], Xiaohua Li[b], Shaojuan Yu[c], Mingyu Sun[d], Boquan Jin[a], Zhujun Zhang[b, *], Kun Yang[a, *]

a Department of Immunology, The Fourth Military Medical University, China; b Key Laboratory of Analytical Chemistry for Life Science of Shaanxi Province, School of Chemistry and Chemical Engineering, Shaanxi Normal University, China; c Department of Cardiology, First Hospital of Xi'an, china; d Brigade of Cadet, The Fourth Military Medical University.

ABSTRACT A novel method for sensitive detection of liver cancer cells using anti-CD155 and anti-CD112 monoclonal antibodies conjugated to ultrabright fluorescent mesoporous silica nanoparticle (FMSN) encapsulating Rhodamine 6G and fluorescein was developed. The diameter of the obtained nanoparticle was 90 nm, and the quantum yield was 69%. Because the emission of fluorescein has a high degree of overlap with the excitation of Rhodamine 6G, and these two dyes were sufficiently close to each other on the nanoparticle, fluorescence resonance energy transfer can occur between these two dyes. This transfer not only maintains the original feature of the nanochannels and the skeletal network of the silica weakening the inner filtering of the dye but also makes the excitation peak of the nanoparticle wider and increases the useful load amount of dye. Because the wider stoke shifts weaken the interference of excitation, the detection sensitivity is enhanced at the same time. The $NaIO_4$

a,* Correspondence to: Department of Immunology, The Fourth Military Medical University, Xi'an 710032, China. Tel 86-29-84779171; Fax 86-29-83253816; e-mail yangkunkun@fmmu.edu.cn. b,* Correspondence to: School of Chemistry and Chemical Engineering, Shaanxi Normal University, Xi'an 710062, China. Tel 86-29-85308184; Fax 86-29-85307774; e-mail zhangzj@snnu.edu.cn.
1 These authors contributed equally to this work.

oxidation method does not use a cross-linker but rather uses covalent immobilization of the monoclonal antibodies on the FMSN. This method can maintain the activity of the monoclonal antibodies more easily than the glutaraldehyde method. These advantages ensure that that nanosensor has high sensitivity and specificity for detecting liver cancer SMMC-7721 and HHCC cells. In vivo imaging experiment also ensured that the biosensor can target tumor tissue in mice.

Keywords: mesoporous silica nanoparticle; fluorescence resonance energy transfer; fluorescence imaging; liver cancer; cluster of differentiation 155; cluster of differentiation 112

1. Introduction

Liver cancers are malignant tumors that grow on the surface or the inside of the liver [1, 2]. Liver tumors are discovered by medical imaging (often by accident) or present themselves symptomatically as an abdominal mass, abdominal pain, jaundice, nausea or liver dysfunction [3]. Liver cancers should not be confused with liver metastases, which are cancers that originate from organs elsewhere in the body and migrate to the liver [4]. Hepatitis C is the primary cause of liver cancer [5]. A 2009 study suggested that l-carnitine deficiency is a risk factor for liver cancer and that l-carnitine supplementation could reduce that risk. Chronic hepatitis B infection can also lead to liver cancer [6].

Human natural killer (NK) cells express a series of activating receptors, such as NKG2D, CD226 and NKp46, that are involved in the recognition and killing of target cells [7]. Among them, CD226 is physically and functionally associated with lymphocyte function-associated antigen-1 (LFA-1) on NK cells and is involved in many key functions of immune cells [8,9]. Studies had shown that both CD155 and CD112 are specific ligands for the CD226 triggering receptor [7,10]. CD155 and CD112 are

constitutively expressed at low levels on epithelial and endothelial cells. However, CD155 and CD112 were recently found to be overexpressed in tumor cell lines and primary tumors, including colorectal carcinoma, glioblastoma, acute myeloid leukemia, myeloma, etc [11-16]. In our preliminary studies we found that CD155 and CD112 were highly expressed by hepatoma cells lines, such as SMMC-7721 and HHCC, indicating that CD155 and CD112 might serve as novel biomarkers for liver cancer cells.

Fluorescence microscopy imaging using fluorescent dyes as markers has wide applications in cytology and histology [17-21]. However, with the demand for increasing detection sensitivity, the disadvantages of fluorescent dyes, such as their low labeling efficiency, poor light stability and relatively low fluorescent intensity, have limited the further development and application of fluorescent microscopy imaging. In the past few years, nanotechnology has shown great promise for use in the field of biology. Many fluorescent nanoparticles, including semiconductor quantum dots [22], fluorescent core-shell nanoparticles [23], polymer fluorescent nanospheres [24], rare earth oxide nanoparticles [25], up-conversion fluorescent nanoparticles [26] and liposome fluorescent nanoparticles [27], have been widely studied previously. Compared with conventional fluorescent dyes, fluorescent nanoparticles have high fluorescence intensity and light stability, are easily marked and prepared and have good biological compatibility. In recent years, functionalized mesoporous silica nanoparticles (MSN) have gained great interest in the biomedical field due to their unique properties, including good monodispersity, a huge surface area that may exceed 1000 $m^2 \cdot g^{-1}$, a tunable and uniform pore system, easy functionalization surfaces, restricted nanospaces, biocompatibility, low cytotoxicity, and high thermal and mechanical stability [28-32].

In this paper, we developed a new type of ultrabright fluorescent mesoporous silica nanoparticle (FMSN) combined with anti-CD155 monoclonal antibodies and with anti-CD112 monoclonal

antibodies for detecting liver cancer SMMC-7721 and HHCC cells, respectively. The FMSNs were synthesized using the three-step hydrolysis method. This method provides hydrophobic groups in the FMSN matrix and prevents dyes from being dissolved by toluene in the process of aminopropyl functionalization. The nanochannels and network skeleton of FMSN immobilized the fluorescent dyes in the matrix, which also isolated the dyes from each other and weakened the inner filter effect, causing fluorescence quenching as compared to fluorescent core-shell silica nanoparticles. The obtained FMSN was 90 nm, and the quantum yield was 69%. We used two types of fluorescent dyes, Rhodamine 6G and fluorescein, which can undergo fluorescence resonance energy transfer with each other. This makes the excitation peak of the nanoparticle wider, increases the fluorescence intensity of the nanoparticle and weakens the interference of excitation. Fluorescence resonance energy transfer was not examined in previous studies of mesoporous silica nanoparticles. For bio-application, the FMSN was modified by anti-CD155 monoclonal antibodies and anti-CD112 monoclonal antibodies by the $NaIO_4$ oxidation method. Because a crosslinker was not used, this method can successfully maintain the activity of antibody. The final detection results demonstrated that CD155 and CD112 on the surface of liver cells could be clearly distinguished by modified FMSNs using fluorescent microscopy imaging. The photostablity of FMSN-targeted cells indicated that the photostablity of FMSN is sufficient for detection experiments. At the same, In vivo imaging experiment was used for characterizing the target-tumor ability of the FMSN biosensor in mice.

2. Experimental

2.1 Materials

Anti-CD112 monoclonal antibodies, anti-CD155 monoclonal antibodies, SMMC-7721 liver cancer

cells, HHCC liver cancer cells and negative cells were prepared by the Department of Immunology if the Fourth Military Medical University, China. Tetraethoxysilane (TEOS), hexadecyl trimethyl ammonium bromide (CTAB), (3-aminopropy1) triethoxysilane (APTES), rhodamine 6G, and fluorescein were purchased from Sigma. Trimethoxy(methyl)silane (MTMS) was obtained from Acros (Belgium). HAc, NaAc, NaCl, Na_2HPO_4, KH_2PO_4, KCl, NaH_2PO_4 and $NH_3 \cdot H_2O$ (28–30 wt. %) were purchased from Xi'an Chemical Reagent Company (Xi'an, China).

PBS buffer (pH 7.1) was prepared by dissolving 1.15 g Na_2HPO_4, 8.0 g NaCl, 0.2 g KH_2PO_4, and 0.2 g KCl in 1 L of water.

2.2 Preparation of amino-functionalized mesoporous silica nanoparticle [23]

The nanoparticles were synthesized as follows: CTAB (0.04 g), glycol (0.7 mL), rhodamine 6G (2 mg) and fluorescein (1.2 mg) were dissolved in 50 mL of water assisted by magnetic force stirring. Then, 2.1 mL of $NH_3 \cdot H_2O$ solution was introduced to the CTAB solution, and the temperature of the mixture was adjusted to 60 ℃. TEOS (0.20 mL) was added dropwise to the surfactant solution over 5 min. The mixture was allowed to react for 0.5 h. Then, MTMS (0.03 mL) and the rhodamine 6G and fluorescein dyes were added to the solution. After stirring for 2.5 h, APTES (0.08 mL) was added to the reaction mixture, and it was stirred for an additional 1.5 h at 60 ℃. The resulting solid crude product was filtered and washed with water. After performing the regular dialysis method, CTAB surfactant, $NH_3 \cdot H_2O$, remaining silica precursors, and dye were removed. The nanoparticles were constituted in approximately 1‰ dispersions using a pH 7.1 ammonia water solution and were examined using a transmission electron microscope (TEM; Hitachi H7000; Kyoto, Japan) to determine size and morphology. The characterization of the fluorescent properties of the nanoparticles was performed

using a fluorospectrophotometer (Hitachi F-4600; Kyoto, Japan).

2.3 Covalent immobilization of monoclonal antibodies onto nanoparticles

The $NaIO_4$ oxidation method was used for modifying the mesoporous silica nanoparticles. The same process was used for the covalent immobilization of both monoclonal antibodies. The procedure was as follows:

A. Oxidation of antibody 1) Four hundred micrograms of monoclonal antibody was dissolved in 70 μL of acetate buffer (0.05 mol/L, pH 4.2). 2) The antibody solution to 140 μL of $NaIO_4$ solution (1.5 mg/mL, pH 4.2). 3) The sample was incubated for 2 h at 4˚C in the dark with constant mixing. 4) The reaction was stopped and the unreacted $NaIO_4$ was removed by an ultrafilter washed with acetate buffer.

B. Coupling to nanoparticles 1) Two micrograms of nanoparticles were washed three times in 5 mL of DPBS solution. 2) After the third wash, the nanoparticles were resuspended in 600 μL of PBS, and complete suspension of the nanoparticles was ensured. 3) The oxidized antibody was added to the nanoparticle suspension gradually, and the solution was allowed to react with constant mixing at 4˚C for 20 h. 4) The nanoparticles were washed and resuspended in 600 μL of PBS. 5) Twenty microliters of $NaBH_4$ solution was added (2 mg/mL, pH 7.6-7.8), and the solution was allowed to react at 4˚C for 2 h in the dark with constant mixing. 6) The nanoparticles were washed three times and then stored at 4˚C in PBS (pH7.6-7.8) until use.

2.4 Cell culture

Both the SMMC-7721 (positive) and HHCC (positive) cell lines were hepatocellular carcinoma

(HCC) cell lines. The negative cell line does not express CD155 or CD112. After careful recovery of the frozen cells, they were maintained in 90% DMEM containing 10% FBS, 100 μg/mL streptomycin and 100 units/mL penicillin in a humidified 5% CO_2–95% air atmosphere at 37˚C.

2.5 Immunofluorescence staining

Before staining, the cells were observed to ensure they were in a good state. The process of immunofluorescence staining of the cells was as follows: 1) The cell suspensions were adjusted to 2×10^5~1×10^6/mL. 2) The cells were washed twice in PBS (3 minutes each time at room temperature) and resuspended in 100 μL PBS. 3) One microliter of the nanosensor suspension was added, and the solution was allowed to react at 4˚C for 40 min. 4) The cells were washed three times in PBS to remove unreacted nanosensors.

2.6 Fluorescence microscopy imaging and FCM analysis

Fluorescence microscopy imaging was performed using an Olympus inverted microscope system (Olympus, Model IX70, Tokyo, Japan) with a 100 W high-pressure mercury lamp (Olympus, Model BH2-RFL-T3, Tokyo, Japan) and CCD (Olympus, Model DP70, Tokyo, Japan). The images were all obtained under the same conditions.

The flow cytometer (FCM) detection was performed in FACSCalibur™ (Becton Dickson, NJ, USA).

2.7 Animal model and in vivo imaging

All animal studies were conducted under a protocol approved by National Institute of Biological Science and Animal Care Research Advisory Committee of Fourth Military Medical University. All

experiments involving mice conducted following the guidelines of the Animal Research Ethics Board of Fourth Military Medical University. Six-week-old BALB/c athymic nude mice were purchased from Peking University Health Science Center and tumors were established by subcutaneously injecting cells of 0.10 mL volume containing 5×10^7 cells/mL media into the right flank of the mice. The tumor sizes were monitored every other day and the animals were subjected to in vivo experiments when the diameter of the tumors reached 6~8 mm (typically 3-4 weeks after inoculation).

The free FMSN, FMSN combined with anti-CD155 antibody and FMSN combined with non-relation antibody were injected to different groups mice by Intravenous injection. The imaging acquisition was performed with in vivo imaging system. And the image processing was performed with IVIS Reagents software.

3. Results and Discussion

3.1 Characterization of mesoporous silica nanoparticles

The FMSNs were prepared by three-step hydrolysis. For this method, CTAB surfactant was used as the structure directing agent. EG can improve structural order and control particle size and morphology. TEOS was the main precursor. MTMS was used for hydrophobic transformation. APTES was used as an amino derivative agent. Fig. 1 shows that the size of the obtained FMSNs was approximately 90 nm. The mesoporous structure also could be observed clearly on the surface of the FMSNs.

In the current study [23], the hydrophobic groups provided by MTMS were helpful for protecting the hydrophobic environment of the silica matrix channels. However, the lack of functional groups in nanoparticles has seriously limited their possible biological applications. To make it possible to use the nanoparticles for biological applications, we added amino groups to them by APTES hydrolysis. In

previous studies, aminopropyl-functionalized FMSNs were prepared by refluxing in anhydrous toluene with 3-aminopropyltrimethoxysilane. The problem with this approach was that the dyes were dissolved by toluene, which severely weakened their fluorescence intensity. TEOS and APTES cohydrolysis effectively stabilized the fluorescence intensity of the dyes. Additionally, the introduction of amino groups had two other effects on the nanoparticles: (1) The FMSNs dispersed in water more easily. Our study found that more than 0.05 ml of APTES allowed the FMSNs to disperse in water. (2) The dispersion of the complex between the nanoparticles and antibodies in the PBS solution was affected. An inappropriate pH value of buffer solution causes physical cohesion due to the electrostatic interaction between the nanoparticles and antibodies, and this greatly affects the recognition of the nanosensors. Thus, we tried including different amounts of APTES to generate a suitable pH for good dispersion of the nanosensors in biological applications. The results showed that the pH value that allowed for proper dispersion of the nanoparticles and antibodies generated by the addition of APTES was alkaline. Finally, we chose 0.08 mL as the appropriate dosage of APTES. Initially, APTES was not hydrolyzed to prevent it from affecting the hydrophobic environment in the nanochannels.

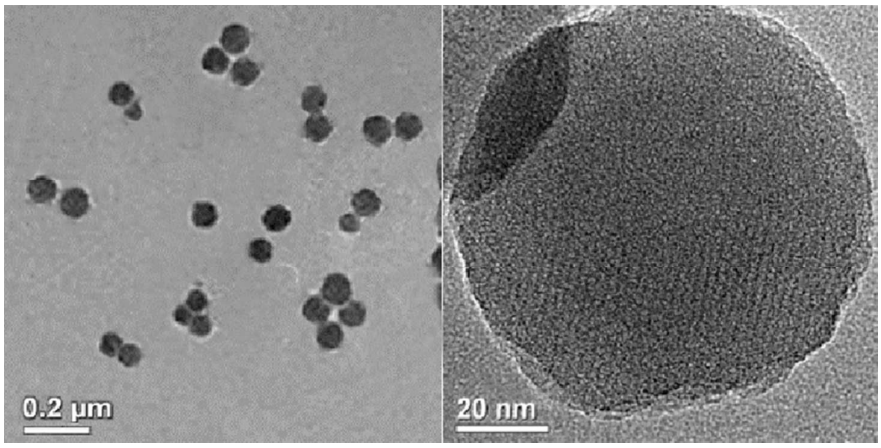

Fig. 1. TEM images of FMSNs. The right figure shows the FMSN has mesoporous structure.

The fluorescence spectra of two dyes and FMSN are shown in Figure 2. It was can be seen that the

maximum emission peaks of free rhodamine 6G and the dye in FMSN were 555 nm and 498 nm, respectively. Compared with rhodamine 6G in solution, the emission peak of FMSN shifted about 7 nm to the left.

The primary conditions to allow for fluorescence resonance energy transfer are as follows: 1. the donor and acceptor molecules must be in close proximity to each other (typically 10-100 Å). The size of the FMSN is 90 ± 20 nm, which can ensure that some dyes will be close enough for fluorescence energy transfer. 2. The absorption or excitation spectrum of the acceptor must overlap the fluorescence emission spectrum of the donor. In Fig. 2, we can see that the emission peak of fluorescein is 518 nm, which greatly overlaps with the excitation of rhodamine 6G.

The phenomenon of the coupling of two emission peaks is possible. In our previous studies, we compared FMSNs with core-shell silica nanoparticles and found several differences between them. In FMSNs, the dyes are loaded into controllable nanochannels or are fixed in the reticular formation, which weakens the interactions of the dyes. This effectively suppresses the inner filtering of the dyes in the FMSNs and increases the useful load amount of the dyes. However, the mesoporous silica matrix cannot completely avoid the inner filtering of the dyes. The results of this study further confirmed this observation. The coupling of emission peaks demonstrated that fluorescence energy transfer did occur between rhodamine 6G and fluorescein. The dyes were fixed within the matrix of the FMSN. Furthermore, some dyes were close enough to each other for energy transfer to occur. This suggests that the distribution of the dyes in matrix is uneven. This phenomenon has two advantages: (1) Coupling widens the excitation peak, which is useful for biological applications. (2) Some fluorescein molecules do not participate in fluorescence energy transfer; thus, their emitted light is not absorbed by rhodamine 6G. This weakens the influence of the inner filtering as compared to when one dye is used.

Additionally, the useful load amounts of dyes were increased, which enhances the fluorescence intensity of the FMSNs. The QY of the FMSNs was 69%.

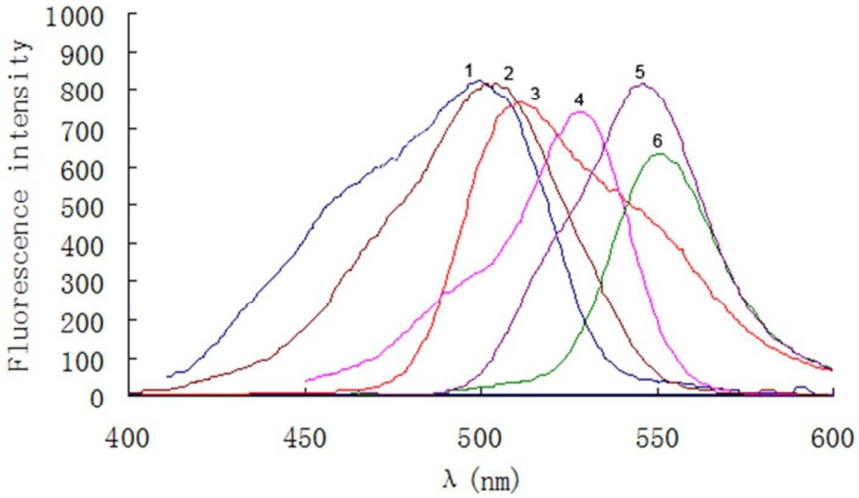

Fig. 2. Fluorescence spectra of dyes and FMSN. 1. The excitation of fluorescein; 2. The excitation of FMSN; 3. The emission of fluorescein; 4. The excitation of rhodamine 6G; 5. The emission of FMSN; 6. The emission of rhodamine 6G.

3.2 Covalent immobilization of monoclonal antibodies onto the surface of FMSN

The $NaIO_4$ method is highly suitable for the modification of FMSNs. The mechanism of this method is as follows: The glycosyl of the glycoprotein is oxidized to an aldehyde group. Then, a Schiff base is formed between the aldehyde group and primary amino group on the nanoparticles. After being deoxidized by $NaBH_4$, the Schiff base turns into a -N=C- bond. In the process of modification, the dihydroxy group of the glycosyl in the Fc segment of the monoclonal antibodies is oxidized to the aldehyde groups by $NaIO_4$ in 4˚C at pH 4.2, and this minimally affects the Fab segment of the antibodies [33]. It should be noted, however, that the $NaIO_4$-oxidized antibody can self-conjugate using its own amines if a high-pH is used. Next, the oxidized antibodies are added to the nanosuspension

gradually to reduce the influence of self-conjugation of the antibodies. After reacting for 20 h, a Schiff base was formed between the aldehyde groups of the antibodies and the amine groups of the nanoparticles. This modification method has three advantages. First, a crosslinker is not introduced in this method, which eliminates the disadvantages of crosslinkers for the activities of antibodies. Secondly, the lack of a crosslinker avoids the dye being dissolved out of the FMSN matrix by the cross-linker during modification processing. Lastly, the fixed reactant ratio and high extent of the reaction resulted in a labeling rate of this modification method of over 50%.

3.3 Detection of liver cancer cells

To ensure consistent measurement conditions, a suitable response time must be determined. Because of the influence of the cells' autofluorescence, the response time for CCD must be selected for fluorescence microscopy imaging. First, positive cells were detected with the CCD mode set to auto. In this mode, the CCD could balance the intensity of the signal and noise to obtain the best quality of imaging. Secondly, other experiments were detected in the conditions that could be fixed in the CCD's configuration.

The fluorescence microscopic images of model cells are shown in Fig. 3. The fluorescence intensity of SMMC-7721 incubated with anti-CD155 nanosensors was the highest of all images. The fluorescence intensities of SMMC-7721 cells incubated with anti-CD112 nanosensors and that of HHCC cells incubated with anti-CD155 nanosensors were roughly the same. The fluorescence intensity of HHCC cells incubated with anti-CD112 nanosensors was the weakest of all of the positive images. Two types of negative cells both showed no fluorescence intensity. These results demonstrated that the expression of CD155 on the cell membrane was higher than that of CD112 in both SMMC-7721 and

HHCC cells. The expressions of both antigens on the SMMC-7721 cell membrane were higher than those on the HHCC cell membrane. This detection experiment proved that the modified FMSN can distinguish the CD155 and CD112 antigens effectively.

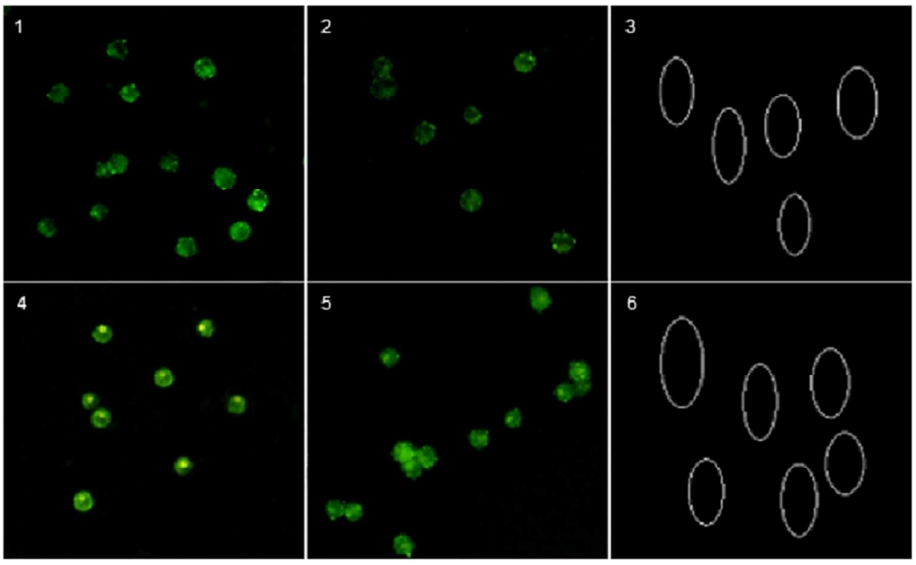

Fig. 3. Fluorescence microscopic imaging. (1) SMMC-7721 cells incubated with anti-CD112 nanosensors; (2) HHCC cells incubated with anti-CD112 nanosensor; (3) Negative cells incubated with anti-CD112 nanosensors; (4) SMMC-7721 cells incubated with anti-CD155 nanosensors; (5) HHCC cells incubated with anti-CD155 nanosensors; (6) Negative cells incubated with anti-CD155 nanosensors.

FCM was also used to detect staining cells (Fig. 4). The results have high consistency with imaging results. The SMMC-7721 cells incubated with anti-CD155 antibodies modified FMSN have highest fluorescence intensity. The fluorescence intensities of FMSN on cells were about ten times as strong as FITC. Furthermore, the peak width of FMSN was wider than peak widths of FITC and blank obviously. This phenomenon is suggested that the signal amplification ability of FMSN was much stronger than FITC.

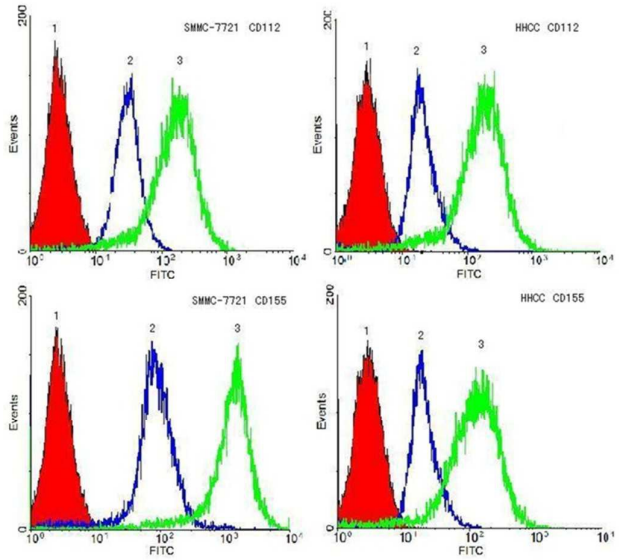

Fig. 4. The results of FCM. 1 Blank cells; 2 Cells incubated with FITC-antibodies; 3 Cells incubated with FMSN-antibodies.

3.4 Photostablity of the FMSN targeting cells

Photobleaching is known to be dependent on solvent interactions and is thought to occur as a bimolecular reaction between a dye and, for example, dissolved oxygen. To investigate the photostability of the modified FMSNs in liver cell detection process, measurements were taken using an Olympus inverted microscope system. After incubating the cells with FMSNs, they were continuously illuminated by a 100 W high-pressure mercury lamp for 60 min, and fluorescence images were acquired every 10 min over a 40 min period. Fig. 5 shows the photobleaching behavior of the anti-CD155 antibody conjugated to FMSN targeting SMMC-7721 cells. The experimental results showed that the fluorescence intensity of the targeting cells clearly change during the 40 min illumination period. This result showed that the FMSN matrix could not isolate the dyes from the surrounding environment. However, the high fluorescence intensity time of FMSNs is sufficient for detecting the cells.

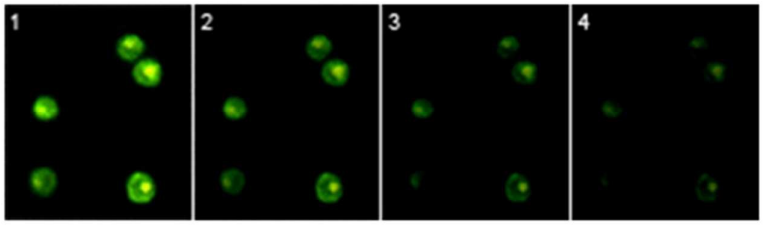

Fig. 5 Photostablity of FMSN in cell membrane. 1. 10 min; 2. 20 min; 3. 30 min; 4. 40 min.

3.5 In vivo imaging

Furthermore, the performance of the FMSN was studied in mice by vivo imaging. Fig. 6 shows the results of in vivo imaging. From the results we can see that the free FMSNs and modified nanosensors can be enriched in lung of mousse. However, the lung enrichment of the free FMSNs are much higher than modified nanosensors. The nanosensors modified anti-CD155 antibody have the lowest enrichment in three groups. It may be explained that the lung tissue contains a lot of macrophages which can phagocytize the nanoparticles. This is the reason why the positive signals were shown in lung. Furthermore, the nanosensors modified anti-CD155 antibody were enriched in tumor tissue obviously. This result points to the nanosensors have the ability of specific recognition to tumor tissue in mice.

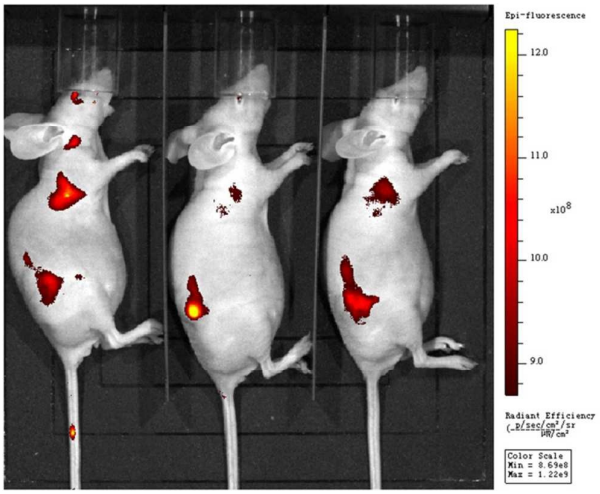

Fig. 6. In vivo imaging of cancer mouse model. 1 free FMSN; 2 FMSN combined with anti-CD155

antibody ; 3 FMSN combined with non-relation antibody.

4. Conclusions

An improved FMSN was prepared using two types of dyes that exhibit fluorescence energy transfer with each other in the FMSN. This improvement maintains the original feature of the FMSN of nanochannels and a skeletal network of silica, which weakens the inner filtering of the dye. At the same, it also widens the excitation peak, increases the useful load amount of the dyes, and broadens the stokes shift to weaken the interference of the excitation. The $NaIO_4$ method can maintain the activities of the antibodies well. The detection results demonstrated that the modified FMSN could distinguish the concentration of antigens on the surface of two types of cells. Additionally, the photobleaching experiment proved that the photostability of the FMSN is sufficient for detecting cells. The in vivo imaging experiment demonstrated that the FMSN biosensor could target tumor tissue in mice.

Acknowledgments

This work was supported financially by the National Natural Science Foundation of China (No. 81171977 and No.31500614), and China Postdoctoral Science Foundation (2014M562598).

References

[1] Douglass HO, Tepper J, Leichman L. Neoplasms of the extrahepatic bile ducts. In: Holland JF, et al, eds. *Cancer Medicine*. Vol 2. Philadelphia, Pa: Lea & Febiger. 1993, 1455-1462.

[2] De Groen PC, Gores GJ, LaRusso NF, et al. Biliary tract cancers. *N Engl J Med*, 1999, 341(18), 1368-1378.

[3] Clary B, Jarnigan W, Pitt H, et al. Hilar cholangiocarcinoma. *J Gastrointest Surg*, Mar-Apr 2004, 8(3), 298-302.

[4] Kuroda T, Rabkin SD, Martuza RL. Effective treatment of tumors with strong beta-catenin/T-cell factor activity by transcriptionally targeted oncolytic herpes simplex virus vector. *Cancer Res*, 2006, 66(20), 10127-10135.

[5] Miao J, Kusafuka T, Udatsu Y, Okada A. Sequence variants of the Axin gene in hepatoblastoma. *Hepatol Res*, 2003, 25(2), 174-179.

[6] Eichenmuller M, Gruner I, Hagl B, et al. Blocking the hedgehog pathway inhibits hepatoblastoma growth. *Hepatology*, 2009, 49(2), 482-490.

[7] Bottino C, Castriconi R, Pende D, et al. Identification of PVR (CD155) and Nectin-2 (CD112) as cell surface ligands for the human DNAM-1 (CD226) activating molecule. *J Exp Med*, 2003, 198, 557-567.

[8] Reymond N, Imbert AM, Devilard E, et al. DNAM-1 and PVR regulate monocyte migration through endothelial junctions. *J Exp Med*, 2004, 199, 1331-1341.

[9] Xu Z, Jin B. A novel interface consisting of homologous immunoglobulin superfamily members with multiple functions. *Cell Mol Immunol*, 2010, 7, 11-19.

[10] Tahara-Hanaoka S, Shibuya K, Onoda Y, et al. Functional characterization of DNAM-1 (CD226) interaction with its ligands PVR (CD155) and nectin-2 (PRR-2/CD112). *Int Immunol*, 2004, 16, 533-538.

[11] El-Sherbiny YM, Meade JL, Holmes TD, et al. The requirement for DNAM-1, NKG2D, and NKp46 in the natural killer cell-mediated killing of myeloma cells. *Cancer Res*, 2007, 67, 8444-8449.

[12] Sloan KE, Eustace BK, Stewart JK, et al. CD155/PVR plays a key role in cell motility during tumor cell invasion and migration. *BMC Cancer*, 2004, 4, 73-86.

[13] Masson D, Jarry A, Baury B, et al. Overexpression of the CD155 gene in human colorectal carcinoma. *Gut*, 2001, 49, 236-240.

[14] Sanchez-Correa B, Gayoso I, Bergua JM, et al. Decreased expression of DNAM-1 on NK cells from acute myeloid leukemia patients. *Immunol Cell Biol*, 2012, 90, 109-115.

[15] Shukla D, Rowe CL, Dong Y, et al. The Murine Homolog (Mph) of Human Herpesvirus Entry Protein B (HveB) Mediates Entry of Pseudorabies Virus but Not Herpes Simplex Virus Types 1 and 2. *J Virol*, 1999, 73(5), 4493-4497.

[16] Lopez M, Aoubala M, Jordier F, et al. The human poliovirus receptor related 2 protein is a new hematopoietic/endothelial homophilic adhesion molecule. *Blood*, 1999, 92(12), 4602-4611.

[17] Hell SW, Stelzer EHK, Lindek S, Cremer C. Confocal microscopy with an increased detection aperture: type-B 4Pi confocal microscopy. *Optics Letters*, 1994, 19(3), 222-224.

[18] Reymann J, Baddeley D, Lemmer P, et al. High precision structural analysis of subnuclear complexes in fixed and live cells via Spatially Modulated Illumination (SMI) microscopy. *Chromosome research*, 2008, 16, 367-382.

[19] Bareyre FM, Garzorz N, Lang C, et al. In vivo imaging reveals a phase-specific role of STAT3 during central and peripheral nervous system axon regeneration. *PNAS*, 2010, 108, 6282-6287.

[20] Bastiaens PIH, Squire A. Fluorescence lifetime imaging microscopy: spatial resolution of biochemical processes in the cell. *Trends in cell biology*, 1999, 9(2), 48-52.

[21] Hess ST, Girirajan TPK, Mason MD. Ultra-High Resolution Imaging by Fluorescence Photoactivation Localization Microscopy. *Biophys J*, 2006, 91(11), 4258-4272.

[22] Deerinck TJ. The Application of Fluorescent Quantum Dots to Confocal, Multiphoton, and Electron Microscopic Imaging. *Toxicol Pathol*, 2008, 36, 112-116.

[23] Tapec R, Zhao XJ, Tan WH. Development of Organic Dye-Doped Silica Nanoparticles for Bioanalysis and Biosensors. *J Nanosci Nanotechnol*, 2002, 2, 405-409.

[24] Hun X, Zhang ZJ, Tao L. Anti-Her-2 monoclonal antibody conjugated polymer fluorescent nanoparticles probe for ovarian cancer imaging. *Anal Chim Acta*, 2008, 625(2), 201-206.

[25] Setua S, Menon D, Asok A, et al. Folate receptor targeted, rare-earth oxide nanocrystals for bi-modal fluorescence and magnetic imaging of cancer cells. *Biomaterials*, 2010, 31(4), 714-729.

[26] Jiang S, Zhang Y, Lim KM, et al. NIR-to-visible upconversion nanoparticles for fluorescent labeling and targeted delivery of siRNA. *Nanotechnology*, 2009, 20, 155101.

[27] Mulder WJ, Strijkers GJ, Habets JW, et al. Storm G.MR molecular imaging and fluorescence microscopy for identification of activated tumor endothelium using a bimodal lipidic nanoparticle. *FASEB J*, 2005, 19(14), 2008-2010.

[28] Slowing I, Trewyn BG, Lin VS. Effect of surface functionalization of MCM-41-type mesoporous silica nanoparticles on the endocytosis by human cancer cells. *J Am Chem Soc*, 2006, 128, 14792-14793.

[29] Zhou H, Wu S, Shen J. Polymer/silica nanocomposites: preparation, characterization, properties, and applications. *Chem Rev*, 2008, 108, 3893-3957.

[30] Slowing I, Trewyn BG, Giri S, et al. Mesoporous silica nanoparticles for drug delivery and biosensing applications. *Adv Funct Mater*, 2007, 17, 1225–1236.

[31] Trewyn BG, Giri S, Slowing I, et al. Mesoporous silica nanoparticle based controlled release, drug delivery, and biosensor systems. Chem Commun, 2007, 3, 3236-3245.

[32] Melde BJ, Johnson BJ. Mesoporous materials in sensing: morphology and functionality at the meso-interface. Anal Bioanal Chem, 2010, 398, 1565-1573.

[33] Abraham R, Moller D, Gabel D, et al. J Immunol Methods, 1991, 144 (1), 77-86.